HHS Public Access

Author manuscript

Toxicol Appl Pharmacol. Author manuscript; available in PMC 2024 November 15.

Published in final edited form as:

Toxicol Appl Pharmacol. 2023 November 15; 479: 116722. doi:10.1016/j.taap.2023.116722.

The Mitochondrial Calcium Uniporter Mediates Mitochondrial Fe^{2+} Uptake and Hepatotoxicity after Acetaminophen

Jiangting Hu[1,2], **Anna-Liisa Nieminen**[1,2,4], **James L. Weemhoff**[5], **Hartmut Jaeschke**[5], **Laura G. Murphy**[1,2], **Judith A. Dent**[1,2], **John J. Lemasters**[1,3,4]

[1]Department of Center for Cell Death, Injury & Regeneration, Medical University of South Carolina, Charleston, SC

[2]Department of Drug Discovery & Biomedical Sciences Medical University of South Carolina, Charleston, SC

[3]Department of Biochemistry & Molecular Biology and Medical University of South Carolina, Charleston, SC

[4]Department of Hollings Cancer Center, Medical University of South Carolina, Charleston, SC

[5]Department of Pharmacology, Toxicology & Therapeutics, University of Kansas Medical Center, Kansas City, KS

Abstract

Acetaminophen (APAP) overdose disrupts hepatocellular lysosomes, which release ferrous iron (Fe^{2+}) that translocates into mitochondria putatively via the mitochondrial calcium uniporter (MCU) to induce oxidative/nitrative stress, the mitochondrial permeability transition (MPT), and hepatotoxicity. To investigate how MCU deficiency affects mitochondrial Fe^{2+} uptake and hepatotoxicity after APAP overdose, global MCU knockout (KO), hepatocyte specific (hs) MCU KO, and wildtype (WT) mice were treated with an overdose of APAP both *in vivo* and *in vitro*. Compared to strain-specific WT mice, serum ALT decreased by 88 and 56%, respectively, in global and hsMCU KO mice at 24 h after APAP (300 mg/kg). Hepatic necrosis also decreased by 84 and 56%. Intravital multiphoton microscopy confirmed loss of viability and mitochondrial depolarization in pericentral hepatocytes of WT mice, which was decreased in MCU KO mice. CYP2E1 expression, hepatic APAP-protein adduct formation, and JNK activation revealed that APAP metabolism was equivalent between WT and MCU KO mice. In cultured hepatocytes after

Address correspondence to: Dr. John J. Lemasters, Medical University of South Carolina, DD504 Drug Discovery Building, 70 President Street, MSC 140, Charleston, SC 29425, Fax: 843-876-2353, JJLemasters@musc.edu.

CREDIT AUTHOR STATEMENT

All authors made a substantial, direct, and intellectual contribution to the work. JH, ALN and JJL contributed to the conception and design of the study. JH, JLW, HJ, LGM and JAD collected the data. All authors contributed to data analysis. JH, ALN and JJL wrote the paper.

Declaration of interests

The authors declare that they have no known competing financial interests or personal relationships that could have appeared to influence the work reported in this paper.

APAP, loss of cell viability decreased in hsMCU KO compared to WT hepatocytes. Using fructose plus glycine to prevent cell killing, mitochondrial Fe^{2+} increased progressively after APAP, as revealed with mitoferrofluor (MFF), a mitochondrial Fe^{2+} indicator. By contrast in hsMCU KO hepatocytes, mitochondrial Fe^{2+} uptake after APAP was suppressed. Rhod-2 measurements showed that Ca^{2+} did not increase in mitochondria after APAP in either WT or KO hepatocytes. In conclusion, MCU mediates uptake of Fe^{2+} into mitochondria after APAP and plays a central role in mitochondrial depolarization and cell death during APAP-induced hepatotoxicity.

Graphical Abstract

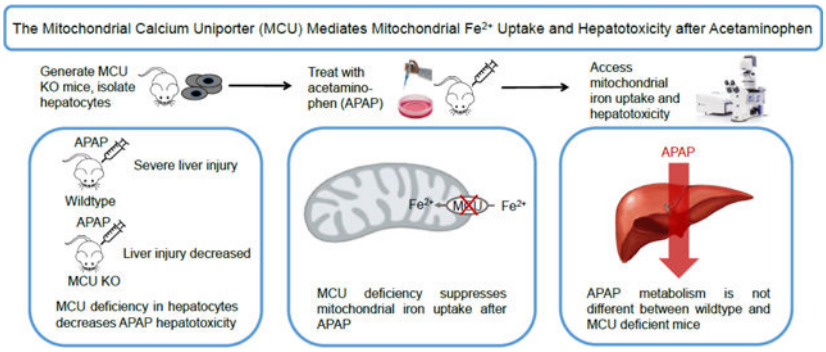

Keywords

APAP; hepatocytes; iron; MCU; mitochondria

1. Introduction

Acetaminophen (APAP) overdose produces severe liver injury, evidenced by serum alanine aminotransferase (ALT) release and hepatic necrosis, and is the leading cause of acute liver failure in North America (Larson, 2007; Hinson et al., 2010). Although extensively studied, the mechanisms of APAP-induced liver injury remain incompletely understood. At a therapeutic dosage, a small portion of APAP is metabolically activated by CYP450 enzymes to generate the toxic metabolite, N-acetyl-p-benzoquinone imine (NAPQI), which is conjugated with and detoxified by GSH (James et al., 2003). With an overdose of APAP, hepatic GSH becomes exhausted, and excess NAPQI leads to oxidative stress, mitochondrial dysfunction, onset of the mitochondrial permeability transition (MPT), and hepatocellular death (Kon et al., 2004; Hanawa et al., 2008).

Iron plays a critical role in oxidative stress in many injuries, including to the liver, heart, and central nervous system (Pucheu et al., 1993; Ghate et al., 2015; Wang et al., 2015). Previous studies identified the lysosomal/endosomal compartment as an important source of mobilizable chelatable iron in the liver (Lemasters, 2004; Kurz et al., 2007; Uchiyama et al., 2008; Kon et al., 2010). The electrogenic mitochondrial Ca^{2+} uniporter (MCU) is a transmembrane protein located in mitochondrial inner membrane, which also can transport Fe^{2+} into mitochondria during oxidative injury to hepatocytes (Flatmark and Romslo, 1975; Uchiyama et al., 2008). Previous studies from our laboratory showed that APAP

disrupts lysosomes, which release ferrous iron (Fe^{2+}) into the cytosol. Cytosolic Fe^{2+} then translocates into mitochondria likely by MCU to induce the MPT and killing in hepatocytes (Hu et al., 2016a; Hu and Lemasters, 2020). Here, to implicate specifically MCU in Fe^{2+} uptake into mitochondria during APAP hepatotoxicity, we used both global MCU knockout (KO) and hepatic specific (hs) MCU KO mice. Both *in vivo* and *in vitro*, MCU deficiency protected against APAP hepatotoxicity after APAP. Protection was associated with blockade of cytosolic iron movement into mitochondria. By contrast, Ca^{2+} did not accumulate inside mitochondria after APAP. Thus, MCU in hepatocytes plays a central role in mitochondria uptake of Fe^{2+} rather than Ca^{2+} after APAP, which drives MPT onset, and cell death.

2. Materials and Methods

2.1. Materials

Rhodamine 123 (Rh123), propidium iodide (PI), Rhod-2 AM and rat anti-F4/80 antibody were purchased from ThermoFisher Scientific (Waltham, MA); RPMI1640 from Gibco (Rockville, MD); glass bottom Petri dishes from MatTek Corp (Ashland, MA); rabbit anti-CYP2E1 antibody (Abcam, Waltham, MA), rabbit anti-MCU, rabbit anti-JNK and anti-phospho-JNK (pJNK) antibodies from Cell Signaling Technology (Danvers, MA); and other reagent grade chemicals from Sigma-Aldrich (St. Louis, MO). Mitoferrofluor (MFF) was synthesized, as described (Kholmukhamedov et al., 2022). When used, MFF was dissolved in dimethyl sulfoxide (DMSO). For experiments, the final concentration of DMSO was 0.1%. Vehicle for other agents was water or hormonally defined medium (HDM). Vehicle controls were performed in all experiments.

2.2. Animals

Male global MCU KO (CD-1 background, Texas A&M Institute for Genomic Medicine, College Station, TX), hsMCU KO (C57BL/6J background), Kupffer cell specific (ks) MCU KO (C57BL/6J background) and WT mice (8–12 weeks) were housed in an environmentally controlled room with a 12-h light/dark cycle and free access to food and water. After overnight fasting, mice were treated with vehicle (warm saline) or APAP (300 mg/kg, i.p.), and food was then made available. All experiments were conducted using animal protocols approved by the Institutional Animal Care and Use Committee.

2.3. Cre-lox breeding strategy and genotyping

To generate hsMCU KO mice, floxed MCU mice (MCU^{fl}, Strain #029817, B6;129s-$Mcu^{tm1.1Jmol}$/J, Jackson Laboratory, Bar Harbor, ME) were mated with alb-cre mice (Jackson Laboratory) to produce double heterozygotes with the floxed MCU (flox) and alb-cre alleles ($MCU^{flox+/-,alb\text{-}cre+/-}$). $MCU^{flox+/-,\ alb\text{-}cre+/-}$ were mated to produce several genotypes, including $MCU^{flox+/+,alb\text{-}cre+/?}$ and $MCU^{flox-/-,alb\text{-}cre\ +/?}$. Hepatocytes of $MCU^{flox+/+,alb\text{-}cre+/?}$ mice become deficient in MCU by an age of 4 weeks when cre recombinase on the albumin promoter begins to be expressed. $MCU^{flox+/+,alb\text{-}cre\ -/-}$ were used as controls. Primers for genotyping of hsMCU KO mice were as follows: for floxed mice, 5’CAG TTA TTC AGT TTA ATG CCG AAG G and 5’GCA AAT GTG CCA GCT TGG T; for alb-cre mice, 5’CCA GGC TAA GTG CCT TCT CTA CA and 5’AAT GCT TCT GTC CGT TTG CCG GT.

Similarly, to generate ksMCU KO mice, MCU^{fl} mice were mated with Clec4f-Cre-tdTomato mice (C57BL/6J-$Clec4f^{em1(cre)Glass}$/J, Strain # 033296, Jackson Laboratory) to produce double heterozygotes with the floxed MCU (flox) and clec4f-cre alleles ($MCU^{flox+/-,cre+/-}$). $MCU^{flox+/-,cre+/-}$ were mated to further produce $MCU^{flox+/+,cre+/?}$ in which MCU is deficient in Kupffer cells. $MCU^{flox+/+,cre-/-}$ were used as controls. Primers for genotyping of ksMCU KO mice were as follows: for floxed mice, 5'CAG TTA TTC AGT TTA ATG CCG AAG G and 5'GCA AAT GTG CCA GCT TGG T; for clec4f-cre mice, 5'ACA CCG GCC TTA TTC CAA G and 5'CAA GAA GTC CAC AGG GTG GT.

2.4. Isolation and Culture of Mouse Hepatocytes

Hepatocytes were isolated from 20 to 25 g overnight-fasted male WT, global MCU KO and, hsMCU KO mice via collagenase perfusion through the inferior vena cava, as described previously (Uchiyama et al., 2008). Hepatocytes were resuspended in Waymouth's medium MB-752/1 containing 2 mM L-glutamine, 10% fetal calf serum, 100 nM insulin, 10 nM dexamethasone, 100 U/ml penicillin, and 100 μg/ml streptomycin, as previously described (Qian et al., 1997). Cell viability was greater than 85% by trypan blue exclusion. Hepatocytes were plated on 0.1% type 1 rat-tail collagen-coated 24-well microtiter plates (1.5×10^5 cells per well) or on glass bottom Petri dishes (3.0×10^5 cells per dish, Maktek Corporation, Ashland, MA). After attaching for 3 h in humidified 5% CO_2, 95% air at 37°C, hepatocytes were washed once and placed in hormonally defined medium (HDM) consisting of RPMI 1640 supplemented with 240 nM insulin, 2 mM L-glutamine, 1 μg/ml transferrin, 0.3 nM selenium, 100 U/ml penicillin, and 100 μg/ml streptomycin at pH 7.4.

2.5. Kupffer cell isolation

Kupffer cells (KCs) were isolated from male WT or ksMCU KO mice via collagenase *in situ* perfusion. In brief, livers were perfused through the inferior vena cava with HBSS, followed by 0.1% collagenase IV (sigma, St Louis, MO). The perfused liver was excised and transferred to a sterile petri dish, then minced with sterile forceps. The homogenized cell suspension was filtered through a 60-μm mesh. Hepatocytes were pelleted by centrifugation at 50 x g for 3 min and the supernatant was collected into a 50 ml conical tube. The cells were washed in HBSS and pelleted by centrifugation at 500 x g for 5 min. The pellet was resuspended in HBSS and layered onto a two layer 25%−50% Percoll gradient (Sigma, St. Louis, MO), and centrifuged at 1800 x g for 15 min with acceleration and brake turned off. Cells in the middle layer were collected and allowed to attach to cell culture plates in DMEM supplemented with 10% FBS and 1% Pen-Strep (Gibco, 15140112) in humidified 5% CO_2, 95% air for 30 min at 37°C. Nonadherent cells were removed by replacing the culture medium.

2.6. Immunocytochemistry

KCs were cultured on glass bottom Petri dishes (4.0×10^4 cells per dish) for 4 h. Subsequently, cells were fixed with 4% paraformaldehyde in phosphate-buffered saline (PBS) for 10 min, permeabilized with 0.2% Triton™ X-100 for 10 min, and blocked with 1% bovine serum albumin (BSA) for 1 h at room temperature. The cells were then labeled with F4/80 monoclonal antibody (ThermoFisher, Waltham, MA) and/or MCU monoclonal antibody (Cell Signaling, Danvers, MA) at 1:100 dilutions in 0.1% BSA, incubated at 4°C

overnight, washed and then incubated with secondary antibody (Alexa Fluor 488 or Alexa Fluor 568, 1:1000) for 1 h at room temperature. Control dishes were probed only with the secondary antibody. After washing with PBS, cells were placed on the stage of a Zeiss LSM 880 laser scanning confocal microscope (White Plains, NY). Green fluorescence Alexa 488 was excited at 488 nm, and emission was collected at 490–560 nm. Red fluorescence Alexa 568 was excited at 559 nm, and emission was imaged at 565–735 nm.

2.7. Fluorometric Assay of Cell Viability

Cell death was assessed using a NovoStar multiwell plate reader (BMG Lab Technologies, Offenburg, Germany), as previously described (Nieminen et al., 1992). Briefly, hepatocytes were incubated in HDM containing 30 μM propidium iodide (PI, ThermoFisher). PI fluorescence from each well was measured at excitation and emission wavelengths of 544 nm and 620 nm (40-nm bandpass), respectively. For each well, fluorescence was first measured at 20 min after addition of PI (Initial) and then at various times after treatment with APAP (X). Experiments were terminated by permeabilizing plasma membranes with 375 μM digitonin. After another 20 min, a final fluorescence measurement (Final) was collected. The percentage of nonviable cells (D) was calculated as D = 100(X -Initial)/ (Final - Initial). Cell killing assessed by PI fluorometry correlates closely with trypan blue exclusion and enzyme release as indicators of oncotic necrosis (Nieminen et al., 1992).

2.8. Loading of fluorophores

For *in vitro* studies, hepatocytes plated on cover glasses were incubated in HDM with 20 mM Na-HEPES buffer (pH 7.4) to maintain pH. In some experiments to stabilize the plasma membrane after APAP exposure and prevent cell death, hepatocytes were incubated with 20 mM fructose plus 5 mM glycine (Kon et al., 2004). To monitor mitochondrial membrane potential ($\Delta\Psi$) and chelatable Fe^{2+}, cells were loaded with 300 nM Rh123 or TMRM ($\Delta\Psi$ indicators) and 1 μM MFF or calcein acetoxymethyl ester (calcein-AM) (Fe^{2+} indicators) for 30 min (Lemasters and Ramshesh, 2007; Kholmukhamedov et al., 2022). Cells were then washed once and incubated in HDM at pH 7.4 containing 100 nM Rh123 but no MFF or 100 nM TMRM and 300 μM calcein free acid. To monitor mitochondrial Ca^{2+}, hepatocytes were loaded with 10 μM Rhod-2 AM for 1 h. Cells were then washed 3 times and incubated in HDM-HEPES at pH 7.4.

2.9. Laser Scanning Confocal Microscopy

Hepatocytes loaded with various combinations of fluorophores were placed in an environmental chamber in 5% CO_2, 95% air at 37°C on the stage of a Zeiss LSM 880 laser scanning confocal microscope (White Plains, NY) equipped with a 63X oil-immersion objective lens. Green fluorescence of Rh123 was excited at 488 nm, and emission was collected at 490–560 nm. Red fluorescence (PI, Rhod-2) was excited at 559 nm, and emission was imaged at 565–735 nm.

2.10. Intravital Multiphoton Microscopy

For intravital microscopy at 24 h after vehicle or APAP injection, mice were anesthetized with ketamine/xylazine and connected to a small animal ventilator via a respiratory tube

(20-gauge catheter) inserted into the trachea. Rh 123 (2 μmol/mouse) plus PI (0.4 μmol/mouse) were infused via polyethylene-10 tubing inserted into the femoral vein over 10 min. After infusion of the fluorescent probes, individual mice were laparotomized and placed in a prone position. The liver was gently withdrawn from the abdominal cavity and placed over a #1.5 glass coverslip mounted on the stage of an inverted Olympus Fluoview 1200 MPE multiphoton microscope (Olympus, Center Valley, PA) equipped with a 60X 1.3 NA silicone oil-immersion objective lens and a Spectra Physics Mai Tai Deep Sea tunable multiphoton laser (Newport, Irvine, CA). Non-descanned green and red fluorescence were separated using 495–540 nm and 575–630 nm band pass filters. Green Rh123 and red PI fluorescence was imaged simultaneously using 800-nm multiphoton excitation. During image acquisition, the respirator was turned off for 5–10 sec to eliminate breathing movement artifacts. Images were collected 25 μm from the liver surface. Pericentral areas were identified by the sinusoidal configuration under the microscope.

2.11. Image Analysis

For *in vitro* studies, Rh123 and MFF fluorescence was quantified using Adobe Photoshop CS4 (San Jose, CA, USA). Briefly, cells were outlined, and mean fluorescence intensity was determined by histogram analysis of the appropriate red and green channels. Background values were obtained from images collected while focusing within the coverslip and were subtracted from mean fluorescence of each field. For *in vivo* studies, punctate green Rh123 fluorescence in hepatocytes represented polarized mitochondria, whereas dimmer diffuse fluorescence signified mitochondrial depolarization. Depolarized areas were quantified in 10 random fields using IP Lab version 3.7 software (BD Biosciences, Rockville, MD) by dividing depolarized areas by total cellular area of the images. Nonviable PI-positive cells, indicated by red nuclear fluorescence, were also counted in ten random fields per liver. Image analysis was performed in a blind fashion.

2.12. Alanine aminotransferase

At 24 h after vehicle or APAP injection, mice were anesthetized with ketamine/xylazine (100 and 10 mg/kg, respectively, i.p.), and blood was collected from the inferior vena cava. Serum ALT was measured using a commercial kit (Pointe Scientific, Canton, MI).

2.13. Histology

Livers were fixed by immersion in 4% paraformaldehyde in PBS. Area percent of necrosis was quantified in hematoxylin and eosin (H&E)-stained paraffin sections with IP Lab software (BD Biosciences, Rockville, MD).

2.14. Western blotting

Protein was extracted from liver tissue, as previously described (Shi et al., 2012). Equivalent amounts of protein were resolved on NuPAGE Bis-Tris 4%−12% polyacrylamide gels, transferred to PVDF membranes, and probed with primary antibodies (1:1000 dilution): rabbit anti-MCU antibody (Danvers, MA), rabbit anti-CYP2E1 antibody, rabbit anti-JNK antibody, rabbit anti-phospho-JNK (pJNK) antibody, and rabbit anti β-actin. The secondary antibody was HRP-conjugated anti-rabbit IgG (1:10000 dilution). Membranes

were developed by the Enhanced Chemiluminescence Detection System (Thermo Fisher Scientific) and imaged using a Caresteam 4000 PRO image station (Woodbridge, CT). Whole gel images and loading controls for Western blots are shown in Suppl. Fig. 1 and 2.

2.15. NAPQI-protein adduct assay

NAPQI-protein adducts were measured using HPLC with electrochemical detection, as previously described (McGill et al., 2012).

2.16. Statistical analysis

Data are presented as means ± standard error. Differences between groups were analyzed by the Student's t-test or ANOVA followed by Tukey's multiple comparison procedure, as appropriate, using $p<0.05$ as the criterion of significance. Images shown are representative of three or more experiments.

3. Results

3.1. Creation of hepatocyte MCU-deficient and Kupffer cell MCU-deficient mice

hsMCU mice were bred by crossing alb-cre mice with floxed MCU mice. Western blots confirmed the absence of MCU protein expression in isolated hepatocytes from both global MCU KO and hsMCU KO mice (Fig. 1A, Suppl. Fig. 1A and 2A). However MCU protein remained expressed in the kidneys of hsMCU KO (Fig. 1B, Suppl. Fig. 1B and 2B). Similarly, ksMCU KO mice were bred by crossing Clec4f-Cre-tdTomato mice with floxed MCU mice. Immunocytochemistry confirmed the absence of MCU protein expression in the KCs of ksMCU KO mice (Fig 1C).

3.2. Decreased acetaminophen-induced ALT release and liver necrosis in global MCU deficient and hepatocyte specific MCU deficient mice but not Kupffer cell specific MCU deficient mice

Liver injury after APAP overdose was assessed from ALT release and necrosis. At 24 h after overdose of APAP (300 mg/kg), serum ALT was 5,166 ± 886 U/L in strain specific WT mice compared to 605 ± 210 U/L in global MCU KO mice (Fig. 2A). From our previous studies, the normal reference range for serum ALT in control mice is 30–35 U/L (Hu et al., 2016b). In vehicle-treated mice, liver histology was normal (Fig. 2B, top, left). At 24 h after APAP, necrosis with a pericentral distribution was 37 ± 7% of cross-sectional areas in strain specific WT mice (Fig. 2B, top right) compared to 6 ± 3% in global MCU knockout mice (Fig. 2B, bottom left).

In hsMCU WT mice (MCU-expressing littermates of hsMCU KO mice), overdose of APAP increased serum ALT to 9,398 ± 3,075 U/L at 24 h, indicating severe liver injury (Fig. 3A). By contrast in hsMCU KO mice, ALT decreased to 4,104 ± 403 U/L after APAP. In hsMCU WT mice, hepatic necrosis was 54 ± 7 % after APAP versus 23 ± 2% in hsMCU KO mice (Fig. 3B, top and bottom left, arrows and Fig. 3C).

To assess the role of MCU in Kupffer cells in APAP-induced hepatotoxicity, we also treated ksMCU KO mice with APAP. However, ALT and hepatic necrosis between ksMCU KO

and the corresponding WT mice at 24 h after overdose APAP were very similar and not statistically significantly different (Fig. 3A, B and C).

3.3. Decreased acetaminophen-induced cell killing in MCU deficient hepatocytes *in vitro*

APAP-induced killing of primary cultured hepatocytes was determined by PI fluorescence assay. When mouse hepatocytes were exposed to 10 mM APAP (toxic dose for mouse hepatocytes *in vitro*), loss of cell viability began at 4 h and increased to 60% and 80% after 6 and 10 h (Fig. 4), as observed previously (Kon et al., 2004). In MCU KO hepatocytes, cell killing was significantly less after APAP at all time points between 4 and 10 h (Fig. 4), confirming an important role for MCU in APAP hepatotoxicity.

3.4. Suppression of mitochondrial iron uptake, mitochondrial depolarization, and cell death in MCU-deficient hepatocytes treated with acetaminophen

To further assess the role of MCU in the translocation of chelatable iron into mitochondria during APAP hepatotoxicity, hsMCU KO and WT mouse hepatocytes were co-loaded with Rh123 and MFF. Rh123 is a cationic, green-fluorescing dye that is an indicator of mitochondrial $\Delta\Psi$. In our previous studies, calcein-AM was used to monitor mitochondrial iron uptake in rat hepatocytes (Uchiyama et al., 2008; Zhang and Lemasters, 2013). However, the cold-loading/warm incubation strategy to load calcein into mitochondria is species-dependent, and mitochondria of mouse hepatocytes label poorly with calcein. Accordingly, MFF was used here to detect mitochondrial Fe^{2+} in mouse hepatocytes. Like Rh123, cationic MFF also accumulates electrophoretically in mitochondria driven by $\Delta\Psi$, but unlike Rh123, MFF binds covalently to sulfhydryls of intramitochondrial proteins and is not released after mitochondrial depolarization. MFF is specific for Fe^{2+} (and Cu^{2+}). Other multivalent cations, including calcium, do not quench MFF (Kholmukhamedov et al., 2022). Increased Fe^{2+} after APAP was distinguished from increased Cu^{2+} using desferal, which chelates iron but not copper (Hu et al., 2016a). In these experiments, 20 mM fructose and 5 mM glycine were added to the medium to prevent plasma membrane permeabilization and necrotic cell death after APAP (Kon et al., 2004). In hsMCU WT hepatocytes treated with APAP, mitochondrial MFF fluorescence was bright at 0 h but subsequently became progressively quenched, beginning within 4 h and becoming virtually complete after 12 h (Fig. 5A and C). Dipyridyl (DPD), an Fe^{2+} chelator, partially restored quenched MFF fluorescence. (Fig. 5A). As mitochondrial Fe^{2+} loading (MFF quenching) progressed, mitochondrial depolarization (loss of Rh123) began to occur at 6 h and was complete within 12 h (Fig. 5A).

By contrast, in hsMCU KO hepatocytes, mitochondrial MFF quenching and mitochondrial depolarization were suppressed after APAP (Fig. 5B). Fluorescence quantification revealed that MFF fluorescence after APAP decreased 30 ± 9% at 12 h in hsMCU KO hepatocytes compared to 84 ± 1 % in the WT hepatocytes (Fig. 5C). By comparison, MFF fluorescence in C57BL/6 WT hepatocytes not treated with APAP decreased 20.4 ± 4% (data not shown). Calculation of Fe^{2+} concentration based on MFF fluorescence is not presently possible and is the topic of future technique development. Rh123 fluorescence after APAP decreased 40 ± 4% at 12 h in hsMCU KO hepatocytes compared to 91 ± 2% in the WT hepatocytes (Fig.

5D). These results indicate that MCU in hepatocytes mediates mitochondrial iron uptake, which leads to depolarization after APAP.

3.5. Mitochondrial Ca^{2+} did not increase in wildtype and MCU-deficient hepatocytes after acetaminophen

To monitor mitochondrial Ca^{2+} uptake during APAP hepatotoxicity, hepatocytes were co-loaded with Rh123 and Rhod-2 AM. The AM ester of Rhod-2 is cationic, which promotes its uptake and de-esterification inside mitochondria. Confocal microscopy of Rh123 and Rhod-2 colocalization confirms the accumulation of Rhod-2 predominantly into mitochondria (Fig. 6). In our previous study, red mitochondrial Rhod-2 fluorescence increased when mitochondrial Ca^{2+} uptake occurred after thapsigargin treatment (Kholmukhamedov et al., 2022). In the present experiments, mitochondrial Rhod-2 fluorescence failed to increase in both hsMCU WT and KO hepatocytes after APAP, indicating that APAP did not increase of mitochondrial Ca^{2+} (Fig. 6). Nonetheless, APAP was causing MCU-dependent mitochondrial dysfunction in MCU-expressing hepatocytes, as shown by depolarization (loss of Rh123 fluorescence) within 6 h after APAP in hsMCU WT hepatocytes (Fig. 6A) but not in hsMCU KO hepatocytes (Fig. 6B). Fluorescence quantification revealed that Rhod-2 fluorescence did not increase in WT hepatocytes after APAP but instead decreased by 64 ± 5% over 10 h (Fig. 6C). By comparison, in hsMCU KO hepatocytes, Rhod-2 fluorescence decreased by 34 ± 7% ($p<0.05$ vs WT) (Fig. 6C). Rh123 fluorescence after APAP decreased 36 ± 2% at 10 h in hsMCU KO hepatocytes compared to 88 ± 3% in the WT hepatocytes (Fig. 6D).

3.6. Increased cytosolic chelatable iron after acetaminophen in MCU-deficient hepatocytes

To investigate whether iron mobilization into the cytosol of MCU-deficient hepatocytes happens during APAP hepatotoxicity, hepatocytes were co-loaded with TMRM and calcein-AM. TMRM is a red-fluorescing indicator of mitochondrial polarization like Rh123 (Chacon et al., 1994). Calcein-AM becomes de-esterified in the cytosol to release calcein free acid. Quenching of calcein fluorescence signifies an increase of cytosolic chelatable Fe^{2+} (Rauen et al., 2004; Uchiyama et al., 2008). When MCU-deficient hepatocytes were exposed to 10 mM APAP, green cytosolic calcein fluorescence decreased 63 ± 6% at 4 h (Fig. 7). A similar decrease of calcein fluorescence after APAP exposure at 4 h was observed previously in wildtype hepatocytes (Kon et al., 2010). Taken together, the MFF and calcein findings show chelatable Fe^{2+} increases in the cytosol but not the mitochondria in MCU-deficient hepatocytes after APAP treatment.

3.7. MCU deficiency does not alter APAP metabolism

CYP2E1 is the principal enzyme responsible for the conversion of APAP to its active hepatotoxic metabolite, NAPQI (Lee et al., 1996). To investigate whether the protective effect against APAP-induced hepatic injury in MCU depletion resulted from decreased CYP2E1 expression, liver extracts were prepared 2 h after 300 mg/kg APAP administration (before development of toxicity) for Western blotting. CYP2E1 expression in both global MCU KO and hsMCU KO mice was similar to WT mice (Fig. 8A and B, Suppl. Fig. 1C and D, Suppl. Fig. 2C and D).

Protein adduct formation is an important initiating event for mitochondrial dysfunction during APAP metabolism (Jaeschke et al., 2012a; Ramachandran and Jaeschke, 2019). Next, we measured APAP-protein adduct formation at 2 h after APAP administration, a time corresponding to the peak of adduct formation (McGill et al., 2012). APAP-protein adducts were undetectable in mice treated with vehicle (data not shown). After APAP administration, APAP-protein adducts increased to 0.36 ± 0.06 and 0.34 ± 0.02 nmol/mg protein in livers of WT and global MCU KO mice, respectively, which was not significantly different (Fig. 8C).

Previous studies showed that APAP activates JNK signaling to promote mitochondrial dysfunction and cell death (Hanawa et al., 2008; Han et al., 2010). Accordingly, we assessed JNK and phospho-JNK (p-JNK) by Western blotting at 2 h after APAP. The ratio of p-JNK/JNK was 0.90 ± 0.01 and 0.89 ± 0.03 after APAP in WT and global MCU KO groups, respectively, which was not statistically significant (Fig 8D and E, Suppl. Fig. 1E and F). In untreated mice, pJNK was virtually undetectable (data not shown) (Hu et al., 2016b).

3.8. Less mitochondrial dysfunction *in vivo* after acetaminophen in MCU-deficient mice compared to wildtype mice

Mitochondria dysfunction is closely related to liver injury (Hu et al., 2016a; Hu et al., 2016b; Ramachandran and Jaeschke, 2019). Therefore, we assessed mitochondrial polarization status *in vivo* by intravital multiphoton microscopy of Rh123 fluorescence at 24 h after vehicle or APAP treatment. In untreated mice, green fluorescence of Rh123 was punctate in virtually all hepatocytes, indicating mitochondrial polarization (Fig. 9, top left), as shown previously (Hu et al., 2016b). In WT mice after APAP treatment, Rh123 staining became diffuse and dim in many hepatocytes, indicating mitochondrial depolarization (Fig. 9, top right, above dashed line). Some nuclei of hepatocytes with depolarized mitochondria became labeled with red-fluorescing PI, signifying loss of cell viability (data not shown). By contrast, in global MCU KO mice after APAP treatment, fewer hepatocytes had depolarized mitochondria (Fig. 9, bottom left, area to left of dashed line). Quantitation of the depolarized areas showed that depolarization increased to 56 ± 5% of cross-sectional area in WT mice after APAP, but in global MCU KO mice the area of mitochondrial depolarization after APAP was 17 ± 4% ($p < 0.01$ vs APAP alone) (Fig. 9, bottom right).

4. Discussion

Acetaminophen (APAP) overdose causes liver injury involving mitochondrial depolarization and onset of the MPT (Kon et al., 2004). The MPT is caused by opening of permeability transition pores in the mitochondrial inner membrane in response to a variety of stimuli, including increased intramitochondrial Ca^{2+} and ROS formation. After MPT onset, immediate mitochondrial depolarization occurs, followed by ATP depletiondependent necrosis (Lemasters et al., 2009).

Iron is a critical catalyst for ROS formation. Previous studies showed that lysosomal disruption after APAP leads to release of Fe^{2+}, which then translocases into mitochondria to promote the MPT and cell death (Kon et al., 2010; Hu et al., 2016a). Ru360 and minocycline are MCU inhibitors and protect cells from chemical hypoxia, ischemia-reperfusion, and

other stresses (Moore, 1971; Saggu et al., 2012; Schwartz et al., 2013; Zhang and Lemasters, 2013). Ru360 and minocycline also prevent cell killing and iron translocation into mitochondria after APAP, suggesting that Fe^{2+} uptake into mitochondria via MCU contributes to APAP hepatotoxicity (Hu et al., 2016a; Hu and Lemasters, 2020).

Here, we used MCU deficient mice to evaluate directly the role of MCU in APAP hepatotoxicity. Cell killing of *in vitro* cultured MCU-deficient hepatocytes after APAP was substantially slower compared to WT hepatocytes, confirming that MCU contributes to APAP hepatotoxicity (Fig. 4). In an *in vivo* global MCU KO mouse model of APAP overdose hepatotoxicity, serum ALT and liver necrosis at 24 h after APAP decreased by about 80%, which indicates that MCU promotes APAP-induced hepatotoxicity *in vivo*. Also in hsMCU KO mice, ALT and hepatic necrosis after APAP were decreased. However, the protection was not as great as in global MCU KO mice. A possible reason is differences in the background of the different MCU-deficient mouse stains, since sensitivity to APAP-induced hepatotoxicity is well established to be strain-dependent (Smith et al., 2016). The background of global MCU KO mice was CD-1, whereas the background of floxed MCU mice, alb-cre mice, and hsMCU KO mice was C57BL/6. Previously, the inbred mouse strain, C57BL/6, was found to be more sensitive to diet-induced liver disease than the outbred CD-1 mice (Fengler et al., 2016; Muhammad-Azam et al., 2019). Similarly, our data showed higher sensitivity of C57BL/6 to APAP, since hsMCU WT mice on a C57BL/6 background had more ALT release and necrosis than global MCU WT mice on a CD-1 background (Fig. 2 and 3). Accordingly, the greater protection against APAP injury in global MCU KO mice than hsMCU KO mice may be due to less injury to protect against in the former. The different strains of mice may also have different levels of iron, which might also lead to different levels of liver injury.

Although APAP metabolism is predominantly in hepatocytes, MCU in other cell types may also contribute to APAP hepatotoxicity. Kupffer cells are liver resident macrophages that are involved in uptake, processing, and export of iron (Scott and Guilliams, 2018). Kupffer cells and other cells of the innate immune system can help propagate and extend APAP liver injury, although this is controversial (Jaeschke et al., 2012b). It was previously shown that deletion of Kupffer cells with clodronate liposomes increased APAP-induced liver injury (Ju et al., 2002). Consistent with these findings, when MCU was knocked out selectively in Kupffer cells, ALT release and necrosis were unchanged after overdose APAP treatment (Fig. 3 C and D). Thus, the difference of liver injury between global MCU KO and hsMCU KO mice cannot be attributed to deficiency of MCU in Kupffer cells of global MCU KO mice.

In prior studies, we showed that APAP causes lysosomal breakdown and leakage, leading to entry of Fe^{2+} into the cytosol, as shown by fluorescence quenching of Fe^{2+}-indicating calcein (Kon et al., 2010). Such quenching signifying increased cytosolic Fe^{2+} also occurred in MCU-deficient hepatocytes after APAP (Fig 7.). To visualize iron mobilization into mitochondria, we used confocal microscopy of a newly developed mitochondrial iron indicator, MFF (Hu et al., 2016a; Kholmukhamedov et al., 2022). MFF is a Fe^{2+}-quenched red-fluorescing cationic dye that accumulates electrophoretically into mitochondria and then binds covalently to proteins. Thus, MFF is retained after mitochondrial depolarization

unlike previous mitochondrial Fe^{2+} indicators. Hence, quenching of red MFF fluorescence is specific for increased mitochondrial chelatable Fe^{2+} independent of $\Delta\Psi$. Suppression of MFF quenching in hsMCU KO hepatocytes compared to WT hepatocytes treated with 10 mM APAP (Fig. 5) is consistent with our previous findings that the MCU inhibitor, Ru360, inhibits mitochondrial MFF quenching after APAP (Hu et al., 2016a). Iron uptake in isolated mitochondria was also observed previously, which was inhibited by Ru360, a blocker of MCU (Flatmark and Romslo, 1975; Schwartz et al., 2013; Sripetchwandee et al., 2014). Overall, these findings show that MCU is an important pathway for iron uptake into mitochondria during APAP hepatotoxicity.

MCU also transports Ca^{2+} into mitochondria. Previous studies reported impaired calcium homeostasis during in APAP-induced hepatotoxicity *in vivo* that is time- and dose dependent (Corcoran et al., 1987) (Burcham and Harman, 1988). Another *in vitro* study showed instead that no sustained change in cytosolic free Ca^{2+} occurs as irreversible APAP-induced toxicity to hepatocytes progresses (Harman et al., 1992). To monitor Ca^{2+} movement into mitochondria in WT and hsMCU KO hepatocytes during APAP hepatotoxicity, we loaded Ca^{2+}-indicating Rhod-2 into mitochondria, again using glycine plus fructose to prevent onset of cell death that might otherwise confound the measurements. In both WT and hsMCU hepatocytes, mitochondrial Rhod-2 fluorescence did not increase after APAP treatment, despite mitochondrial depolarization, a consequence of MPT onset, as visualized with Rh123. Rhod-2 fluorescence also did not increase in hsMCU KO hepatocytes after 10 mM APAP, indicating that 10 mM APAP did not increase mitochondrial Ca^{2+} in either WT or KO hepatocytes (Fig. 6). Thus, protection against APAP-induced mitochondrial dysfunction in MCU-deficient hepatocytes was mainly related to the blockage of iron movement into mitochondria.

Previous studies showed that APAP overdose increases the proportion of APAP metabolized to NAPQI by cytochrome P450 2E1 (CYP2E1) (Ramachandran and Jaeschke, 2019). NAPQI can be detoxified by glutathione, but after an overdose excessive NAPQI binds to mitochondrial proteins to form APAP protein adducts that trigger an initial oxidant stress (Nguyen et al., 2021), which cause the amplification of ROS and peroxynitrite formation in mitochondria as a crucial step in APAP-induced hepatotoxicity (Saito et al., 2010). Therefore, we explored whether the decreased APAP hepatotoxicity in MCU KO and hsMCU KO mice was due to an alteration of APAP metabolism. At 2 h after APAP before onset of hepatocellular necrosis, CYP2E1 expression in MCU KO and hsMCU KO liver extracts was comparable to WT livers (Fig. 8A and B). APAP protein adducts were undetectable in untreated control mice (data not shown) but became markedly increased at 2 h after APAP treatment. Notably, APAP protein adduct formation did not decrease in MCU-deficient livers (Fig. 8C). Thus, MCU deficiency does not alter hepatic APAP metabolism.

JNK activation is also involved in APAP-induced liver injury due to increased ROS generation. Activated pJNK translocates to mitochondria during APAP hepatotoxicity, an event that further enhances ROS generation and contributes to MPT onset and cell death (Hanawa et al., 2008). Our data confirmed that early JNK activation occurred at 2 h after APAP in WT mice. However, MCU deficiency did not significantly alter JNK activation

(Fig. 8D and E). Thus, decreased APAP hepatotoxicity in MCU-deficient mice cannot be explained by inhibition of JNK activation or any other event upstream of mitochondria.

Previous studies implicated that MPT is an important mechanism underlying mitochondrial dysfunction in APAP-induced hepatotoxicity (Kon et al., 2004; Reid et al., 2005). Toxic doses of APAP induce mitochondrial depolarization both in cultured mouse hepatocytes and *in vivo* in mouse livers (Kon et al., 2004; Hu et al., 2016b). The iron chelator, starch-desferal, and the MCU inhibitor, minocycline, decreased hepatic mitochondrial depolarization and cell death *in vivo* in mice after APAP, suggesting that the MPT is likely triggered by iron uptake into mitochondria through MCU (Hu and Lemasters, 2020). Here using intravital multiphoton microscopy, we showed that mitochondrial depolarization decreased in MCU-deficient mice compared to WT mice at 24 h after 300 mg/kg APAP administration (Fig. 9), results that confirm and extend the conclusion that MCU plays an important role in hepatic mitochondrial dysfunction induced by overdose of APAP.

The key question how the mitochondrial uptake of Fe^{2+} mediates the MPT remains to be answered. In general, Fe^{2+} is considered a catalyst for the Fenton reaction and initiation of lipid peroxidation (LPO). However, the extent of LPO is limited after APAP overdose and considered insufficient to cause cell death (Du et al., 2016). In contrast, there is strong evidence for formation of peroxynitrite, a reaction product of the superoxide radical and the nitric oxide radical, selectively in the mitochondrial matrix (Cover et al., 2005). Direct experimental support for the critical role of peroxynitrite in APAP-induced cell death comes from the observation that partial Mn-SOD-deficient mice showed a dramatic increase in injury compared to WT animals (Ramachandran et al., 2011) and that mitochondria-specific SOD mimetics eliminated nitrotyrosine protein adducts and prevented APAP-induced liver injury (Du et al., 2017; He et al., 2023). Based on these findings, it was shown that iron chelation blocked nitrotyrosine formation and effectively protected against APAP hepatotoxicity independent of LPO (Adelusi et al., 2022), which is consistent with Fe^{2+} acting as a catalyst for peroxynitrite-mediated protein nitration (Campolo et al., 2014). Thus, under normal circumstances mitochondrial Fe^{2+} uptake promotes mitochondrial dysfunction through protein nitration not LPO (Adelusi et al., 2022). However, in case of an iron overload, both Fe^{2+}-catalyzed protein nitration and LPO contribute to the MPT and cell death (Adelusi et al., 2022).

Taken together, our results indicate that MCU mediates translocation into mitochondria of Fe^{2+} released from lysosomes after APAP. Fe^{2+} entering mitochondria via MCU promotes mitochondrial depolarization due to the MPT, bioenergetic failure, and ultimately hepatocellular death. Although MCU is a transporter of Ca^{2+}, protection afforded by MCU deficiency against APAP could not be attributed to inhibition of mitochondrial Ca^{2+} uptake. Future studies will focus on development and optimizing conditions for drugs that target MCU to minimize APAP hepatotoxicity.

Supplementary Material

Refer to Web version on PubMed Central for supplementary material.

ACKNOWLEDGMENTS

This work was supported, in part, by grants AA021191, AA025379, AA022815, DK073336, DK119523, DK102142, ES031335, and UL1 TR001450 from the National Institutes of Health, United States. Imaging and spectroscopy facilities were supported, in part, by P20 GM130457, P30 CA138313, P30 DK123704, P30 GM140964, P30 GM118247, and 1 S10 OD018113.

Abbreviations:

•OH	hydroxyl radical
ΔΨ	membrane potential
ALT	alanine aminotransferase
APAP	acetaminophen
BSA	bovine serum albumin
DPD	dipyridyl
GSH	glutathione
HDM	hormonally defined medium
MCU	mitochondrial calcium uniporter
MFF	mitoferrofluor
MPT	mitochondrial permeability transition
NAPQI	*N*-acetyl-*p*-benzoquinone imine
PBS	phosphate-buffered saline
PI	propidium iodide
PT	permeability transition
Rh123	rhodamine 123
ROS	reactive oxygen species

References

Adelusi OB, Ramachandran A, Lemasters JJ, Jaeschke H, 2022. The role of iron in lipid peroxidation and protein nitration during acetaminophen-induced liver injury in mice. Toxicol Appl Pharmacol 445: 116043.

Burcham PC, Harman AW, 1988. Effect of acetaminophen hepatotoxicity on hepatic mitochondrial and microsomal calcium contents in mice. Toxicol Lett 44, 91–99. [PubMed: 3188086]

Chacon E, Reece JM, Nieminen AL, Zahrebelski G, Herman B, Lemasters JJ, 1994. Distribution of electrical potential, pH, free Ca2+, and volume inside cultured adult rabbit cardiac myocytes during chemical hypoxia: a multiparameter digitized confocal microscopic study. Biophys J 66, 942–952. [PubMed: 8038398]

Corcoran GB, Wong BK, Neese BL, 1987. Early sustained rise in total liver calcium during acetaminophen hepatotoxicity in mice. Res Commun Chem Pathol Pharmacol 58, 291–305. [PubMed: 3438568]

Fengler VH, Macheiner T, Kessler SM, Czepukojc B, Gemperlein K, Muller R, Kiemer AK, Magnes C, Haybaeck J, Lackner C, Sargsyan K, 2016. Susceptibility of Different Mouse Wild Type Strains to Develop Diet-Induced NAFLD/AFLD-Associated Liver Disease. PLoS One 11, e0155163.

Flatmark T, Romslo I, 1975. Energy-dependent accumulation of iron by isolated rat liver mitochondria. Requirement of reducing equivalents and evidence for a unidirectional flux of Fe(II) across the inner membrane. J Biol Chem 250, 6433–6438. [PubMed: 808543]

Ghate NB, Chaudhuri D, Das A, Panja S, Mandal N, 2015. An Antioxidant Extract of the Insectivorous Plant Drosera burmannii Vahl. Alleviates Iron-Induced Oxidative Stress and Hepatic Injury in Mice. PLoS One 10, e0128221.

Han D, Shinohara M, Ybanez MD, Saberi B, Kaplowitz N, 2010. Signal transduction pathways involved in drug-induced liver injury. Handb Exp Pharmacol, 267–310.

Hanawa N, Shinohara M, Saberi B, Gaarde WA, Han D, Kaplowitz N, 2008. Role of JNK translocation to mitochondria leading to inhibition of mitochondria bioenergetics in acetaminophen-induced liver injury. J Biol Chem 283, 13565–13577. [PubMed: 18337250]

Harman AW, Mahar SO, Burcham PC, Madsen BW, 1992. Level of cytosolic free calcium during acetaminophen toxicity in mouse hepatocytes. Mol Pharmacol 41, 665–670. [PubMed: 1569920]

Hinson JA, Roberts DW, James LP, 2010. Mechanisms of acetaminophen-induced liver necrosis. Handb Exp Pharmacol, 369–405.

Hu J, Kholmukhamedov A, Lindsey CC, Beeson CC, Jaeschke H, Lemasters JJ, 2016a. Translocation of iron from lysosomes to mitochondria during acetaminophen-induced hepatocellular injury: Protection by starch-desferal and minocycline. Free Radic Biol Med 97, 418–426. [PubMed: 27345134]

Hu J, Lemasters JJ, 2020. Suppression of iron mobilization from lysosomes to mitochondria attenuates liver injury after acetaminophen overdose in vivo in mice: Protection by minocycline. Toxicol Appl Pharmacol 392, 114930.

Hu J, Ramshesh VK, McGill MR, Jaeschke H, Lemasters JJ, 2016b. Low Dose Acetaminophen Induces Reversible Mitochondrial Dysfunction Associated with Transient c-Jun N-Terminal Kinase Activation in Mouse Liver. Toxicol Sci 150, 204–215. [PubMed: 26721299]

Jaeschke H, McGill MR, Ramachandran A, 2012a. Oxidant stress, mitochondria, and cell death mechanisms in drug-induced liver injury: lessons learned from acetaminophen hepatotoxicity. Drug Metab Rev 44, 88–106. [PubMed: 22229890]

Jaeschke H, Williams CD, Ramachandran A, Bajt ML, 2012b. Acetaminophen hepatotoxicity and repair: the role of sterile inflammation and innate immunity. Liver Int 32, 8–20. [PubMed: 21745276]

James LP, Mayeux PR, Hinson JA, 2003. Acetaminophen-induced hepatotoxicity. Drug Metab Dispos 31, 1499–1506. [PubMed: 14625346]

Kholmukhamedov A, Li L, Lindsey CC, Hu J, Nieminen AL, Takemoto K, Beeson GC, Beneker CM, McInnes C, Beeson CC, Lemasters JJ, 2022. A new fluorescent sensor mitoferrofluor indicates the presence of chelatable iron in polarized and depolarized mitochondria. J Biol Chem 298, 102336.

Kon K, Kim JS, Jaeschke H, Lemasters JJ, 2004. Mitochondrial permeability transition in acetaminophen-induced necrosis and apoptosis of cultured mouse hepatocytes. Hepatology 40, 1170–1179. [PubMed: 15486922]

Kon K, Kim JS, Uchiyama A, Jaeschke H, Lemasters JJ, 2010. Lysosomal iron mobilization and induction of the mitochondrial permeability transition in acetaminophen-induced toxicity to mouse hepatocytes. Toxicol Sci 117, 101–108. [PubMed: 20584761]

Kurz T, Terman A, Brunk UT, 2007. Autophagy, ageing and apoptosis: the role of oxidative stress and lysosomal iron. Arch Biochem Biophys 462, 220–230. [PubMed: 17306211]

Larson AM, 2007. Acetaminophen hepatotoxicity. Clin Liver Dis 11, 525–548, vi. [PubMed: 17723918]

Lee SS, Buters JT, Pineau T, Fernandez-Salguero P, Gonzalez FJ, 1996. Role of CYP2E1 in the hepatotoxicity of acetaminophen. J Biol Chem 271, 12063–12067. [PubMed: 8662637]

Lemasters JJ, 2004. Rusty notions of cell injury. J Hepatol 40, 696–698. [PubMed: 15030988]

Lemasters JJ, Ramshesh VK, 2007. Imaging of mitochondrial polarization and depolarization with cationic fluorophores. Methods Cell Biol 80, 283–295. [PubMed: 17445700]

Lemasters JJ, Theruvath TP, Zhong Z, Nieminen AL, 2009. Mitochondrial calcium and the permeability transition in cell death. Biochim Biophys Acta 1787, 1395–1401. [PubMed: 19576166]

McGill MR, Williams CD, Xie Y, Ramachandran A, Jaeschke H, 2012. Acetaminophen-induced liver injury in rats and mice: comparison of protein adducts, mitochondrial dysfunction, and oxidative stress in the mechanism of toxicity. Toxicol Appl Pharmacol 264, 387–394. [PubMed: 22980195]

Moore CL, 1971. Specific inhibition of mitochondrial Ca++ transport by ruthenium red. Biochem Biophys Res Commun 42, 298–305. [PubMed: 4250976]

Muhammad-Azam F, Nur-Fazila SH, Ain-Fatin R, Mustapha Noordin M, Yimer N, 2019. Histopathological changes of acetaminophen-induced liver injury and subsequent liver regeneration in BALB/C and ICR mice. Vet World 12, 1682–1688. [PubMed: 32009746]

Nieminen AL, Gores GJ, Bond JM, Imberti R, Herman B, Lemasters JJ, 1992. A novel cytotoxicity screening assay using a multiwell fluorescence scanner. Toxicol Appl Pharmacol 115, 147–155. [PubMed: 1641848]

Pucheu S, Coudray C, Tresallet N, Favier A, de Leiris J, 1993. Effect of iron overload in the isolated ischemic and reperfused rat heart. Cardiovasc Drugs Ther 7, 701–711. [PubMed: 8241014]

Qian T, Nieminen AL, Herman B, Lemasters JJ, 1997. Mitochondrial permeability transition in pH-dependent reperfusion injury to rat hepatocytes. Am J Physiol 273, C1783–1792. [PubMed: 9435481]

Ramachandran A, Jaeschke H, 2019. Acetaminophen Hepatotoxicity. Semin Liver Dis 39, 221–234. [PubMed: 30849782]

Rauen U, Petrat F, Sustmann R, de Groot H, 2004. Iron-induced mitochondrial permeability transition in cultured hepatocytes. J Hepatol 40, 607–615. [PubMed: 15030976]

Reid AB, Kurten RC, McCullough SS, Brock RW, Hinson JA, 2005. Mechanisms of acetaminophen-induced hepatotoxicity: role of oxidative stress and mitochondrial permeability transition in freshly isolated mouse hepatocytes. J Pharmacol Exp Ther 312, 509–516. [PubMed: 15466245]

Saggu S, Hung HI, Quiogue G, Lemasters JJ, Nieminen AL, 2012. Lysosomal signaling enhances mitochondria-mediated photodynamic therapy in A431 cancer cells: role of iron. Photochem Photobiol 88, 461–468. [PubMed: 22220628]

Saito C, Lemasters JJ, Jaeschke H, 2010. c-Jun N-terminal kinase modulates oxidant stress and peroxynitrite formation independent of inducible nitric oxide synthase in acetaminophen hepatotoxicity. Toxicol Appl Pharmacol 246, 8–17. [PubMed: 20423716]

Schwartz J, Holmuhamedov E, Zhang X, Lovelace GL, Smith CD, Lemasters JJ, 2013. Minocycline and doxycycline, but not other tetracycline-derived compounds, protect liver cells from chemical hypoxia and ischemia/reperfusion injury by inhibition of the mitochondrial calcium uniporter. Toxicol Appl Pharmacol 273, 172–179. [PubMed: 24012766]

Scott CL, Guilliams M, 2018. The role of Kupffer cells in hepatic iron and lipid metabolism. J Hepatol 69, 1197–1199. [PubMed: 30001821]

Shi Y, Rehman H, Ramshesh VK, Schwartz J, Liu Q, Krishnasamy Y, Zhang X, Lemasters JJ, Smith CD, Zhong Z, 2012. Sphingosine kinase-2 inhibition improves mitochondrial function and survival after hepatic ischemia-reperfusion. J Hepatol 56, 137–145. [PubMed: 21756852]

Smith AK, Petersen BK, Ropella GE, Kennedy RC, Kaplowitz N, Ookhtens M, Hunt CA, 2016. Competing Mechanistic Hypotheses of Acetaminophen-Induced Hepatotoxicity Challenged by Virtual Experiments. PLoS Comput Biol 12, e1005253.

Sripetchwandee J, KenKnight SB, Sanit J, Chattipakorn S, Chattipakorn N, 2014. Blockade of mitochondrial calcium uniporter prevents cardiac mitochondrial dysfunction caused by iron overload. Acta physiologica (Oxford, England) 210, 330–341. [PubMed: 24034353]

Uchiyama A, Kim JS, Kon K, Jaeschke H, Ikejima K, Watanabe S, Lemasters JJ, 2008. Translocation of iron from lysosomes into mitochondria is a key event during oxidative stress-induced hepatocellular injury. Hepatology 48, 1644–1654. [PubMed: 18846543]

Wang YQ, Wang MY, Fu XR, Peng Y, Gao GF, Fan YM, Duan XL, Zhao BL, Chang YZ, Shi ZH, 2015. Neuroprotective effects of ginkgetin against neuroinjury in Parkinson's disease model induced by MPTP via chelating iron. Free Radic Res 49, 1069–1080. [PubMed: 25968939]

Zhang X, Lemasters JJ, 2013. Translocation of iron from lysosomes to mitochondria during ischemia predisposes to injury after reperfusion in rat hepatocytes. Free Radic Biol Med 63, 243–253. [PubMed: 23665427]

- Mitochondrial calcium uniporter (MCU) deficiency decreases acetaminophen (APAP) liver injury
- MCU deficiency suppresses mitochondrial iron uptake after APAP
- Mitochondrial Ca^{2+} does not increase after APAP
- APAP metabolism is not different between wildtype and MCU deficient mice
- Mitochondrial Fe^{2+} uptake via MCU is in the chain of causation leading to APAP hepatotoxicity

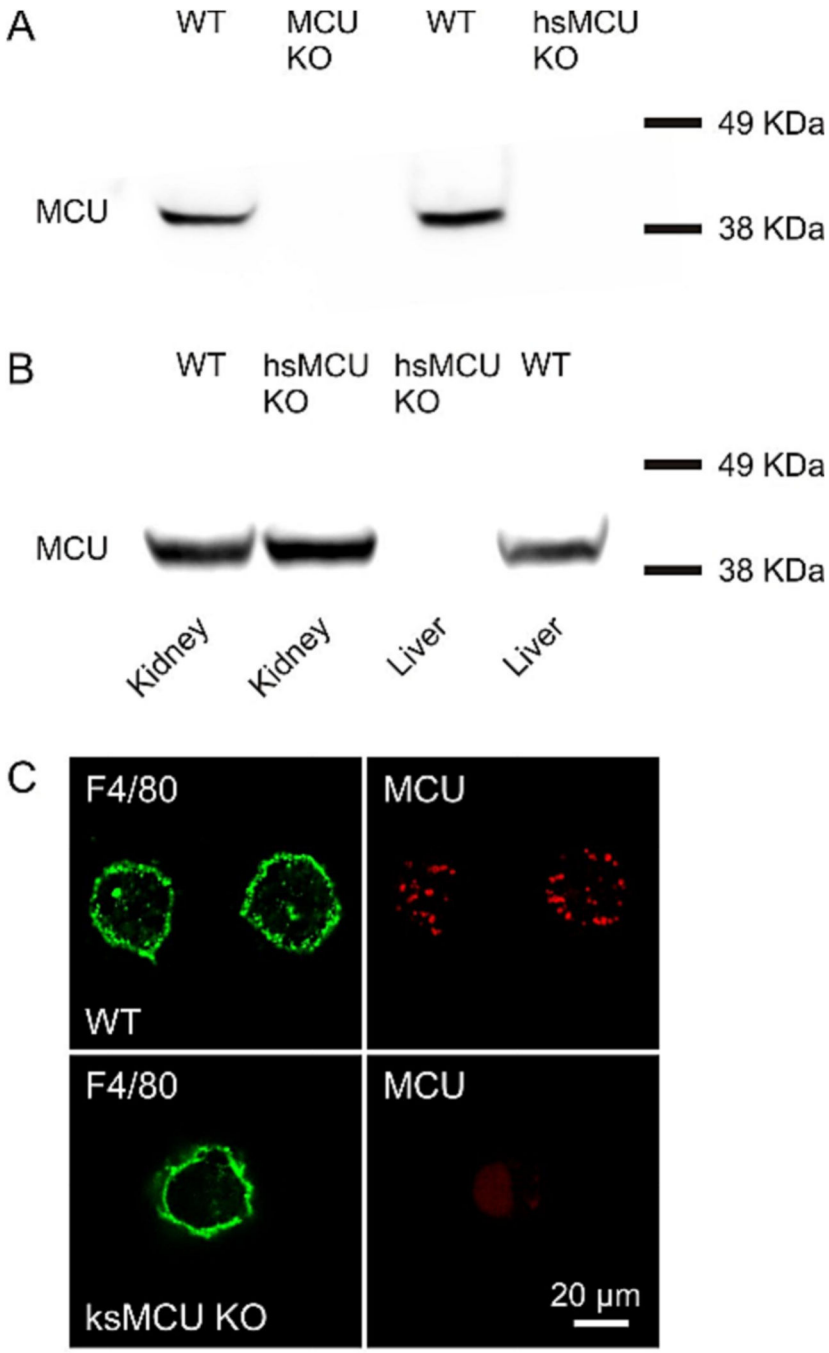

Fig. 1. MCU expression in global, hepatocyte specific and Kupffer cell specific MCU knockout mice.

In A, hepatocytes from hsMCU KO, global MCU KO, and WT mice were examined by Western blotting for MCU expression. **In B**, liver and kidney tissue from hsMCU KO and WT mice were examined by Western blotting for MCU expression. MCU was undetectable in hepatocytes from both hsMCU KO and global MCU KO livers (**A).** MCU protein expression in kidney was not different in hsMCU KO mice compared to corresponding WT mice (**B**). In **C**, Kupffer cells were isolated from WT or ksMCU KO mice, as described in

Materials and Methods. Fluorescence immune-cytochemistry with antibodies against MCU and F4/80 (macrophage/Kupffer cell marker) was performed. MCU antibody showed MCU expression in Kupffer cells of WT mice (top row) but not ksMCU KO mice (bottom row).

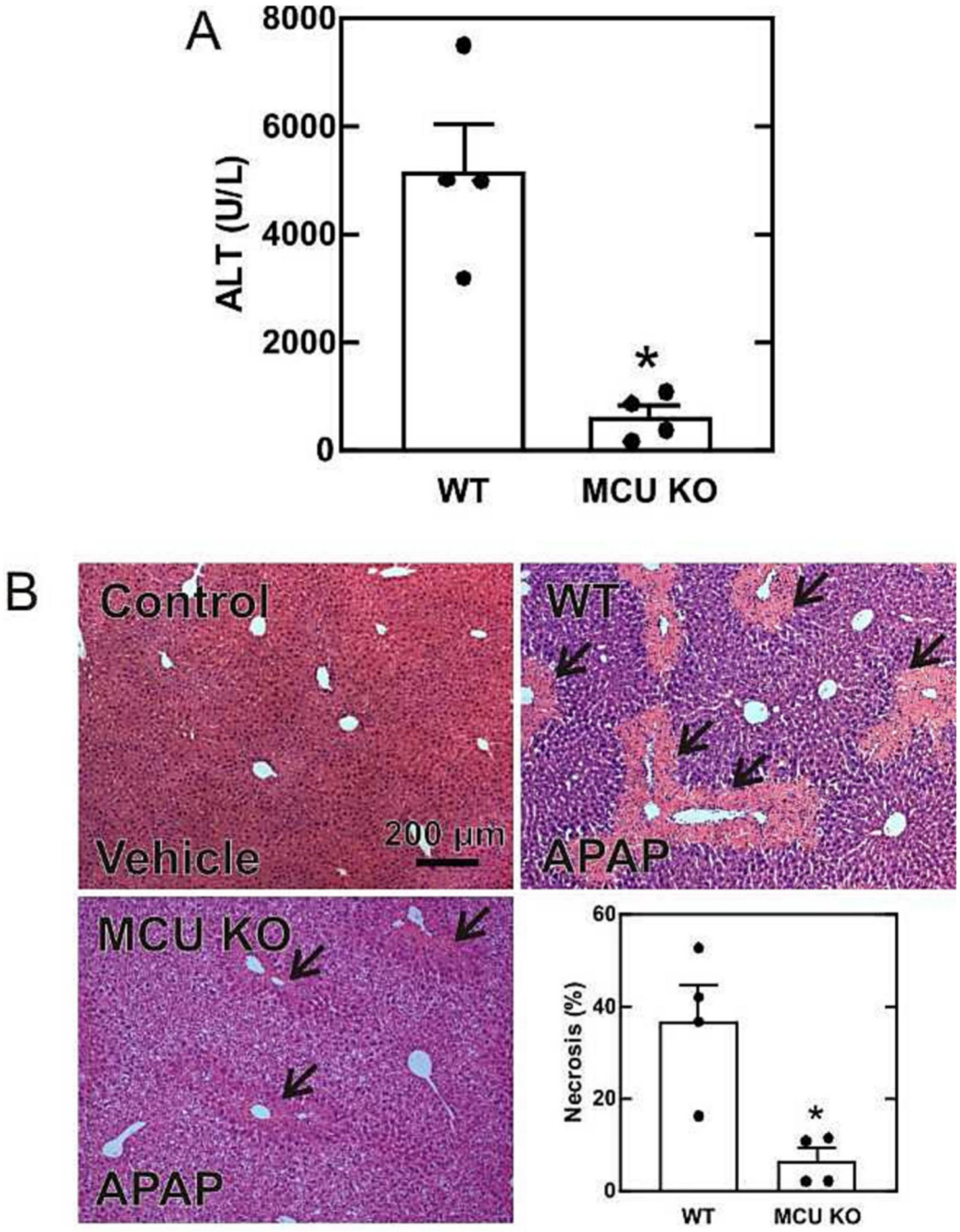

Fig. 2. Serum ALT and liver necrosis decreased in global MCU-deficient mice compared to wildtype mice after acetaminophen administration.

Mice were administered 300 mg/kg APAP or vehicle, as described in Materials and Methods. Serum ALT (**A**) and liver necrosis (**B**) were assessed at 24 h after APAP. Values are means ± SE from four or more mice per group. Black arrows identify necrotic areas. Area percent of necrosis was quantified in liver sections by image analysis of 10 random fields per liver. Necrosis in the vehicle-treated group was absent and not plotted. *, $p < 0.01$ vs WT group.

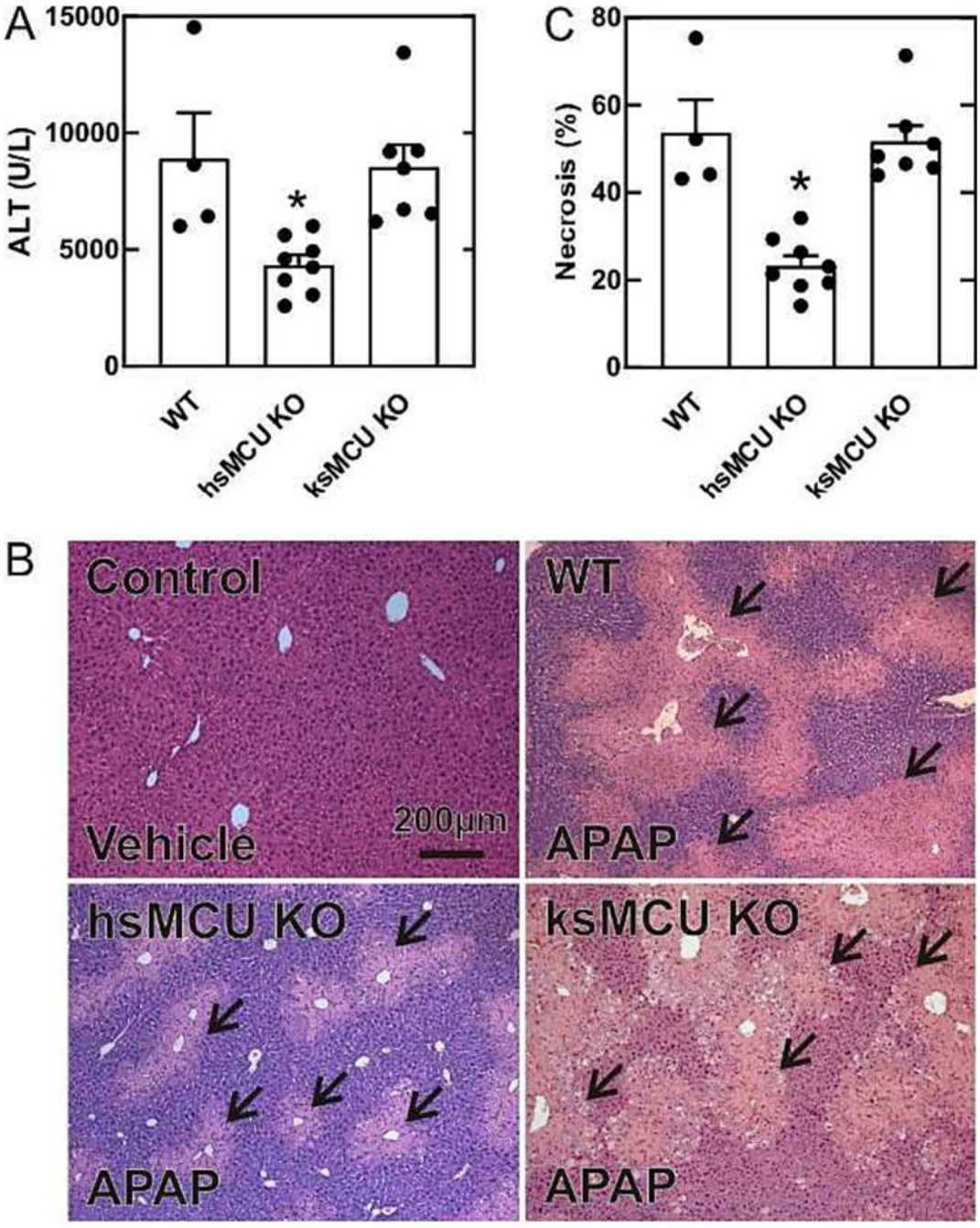

Fig. 3. Serum ALT and liver necrosis in hepatocyte specific MCU-deficient and Kupffer cell specific MCU-deficient mice compared to wildtype mice after acetaminophen administration.

Mice were treated with 300 mg/kg APAP or vehicle, as described in Materials and Methods. Serum ALT (A) and liver necrosis (B and C) were assessed at 24 h after APAP. Values are means ± SE from four or more mice per group. Black arrows identify necrotic areas. Area percent of necrosis was quantified in liver sections by image analysis of 10 random fields per liver. Necrosis in vehicle group was absent and not plotted. *, $p < 0.01$ vs WT group.

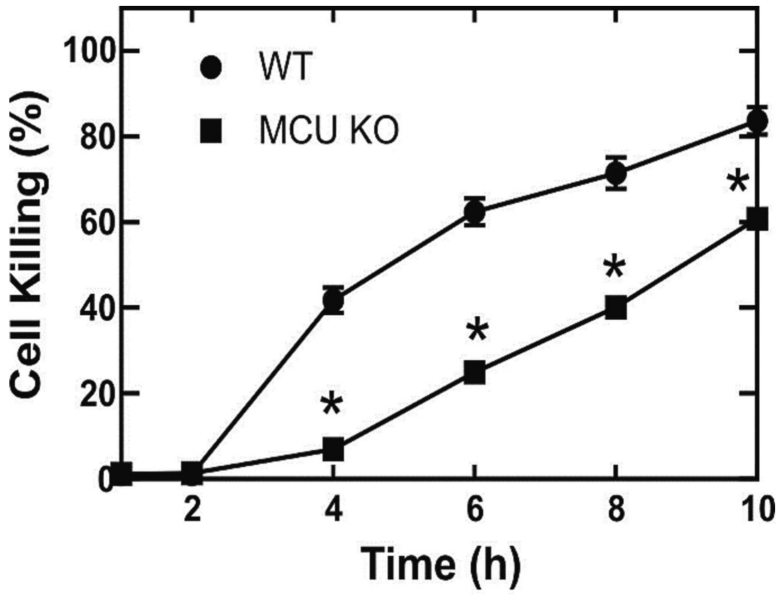

Fig.4. Acetaminophen-induced cell killing in wildtype and global MCU deficient mouse hepatocytes.

WT and global MCU KO mouse hepatocytes were exposed to 10 mM APAP. Cell viability was determined by PI fluorometry. *, $p<0.05$ vs. WT from 3 independent isolations.

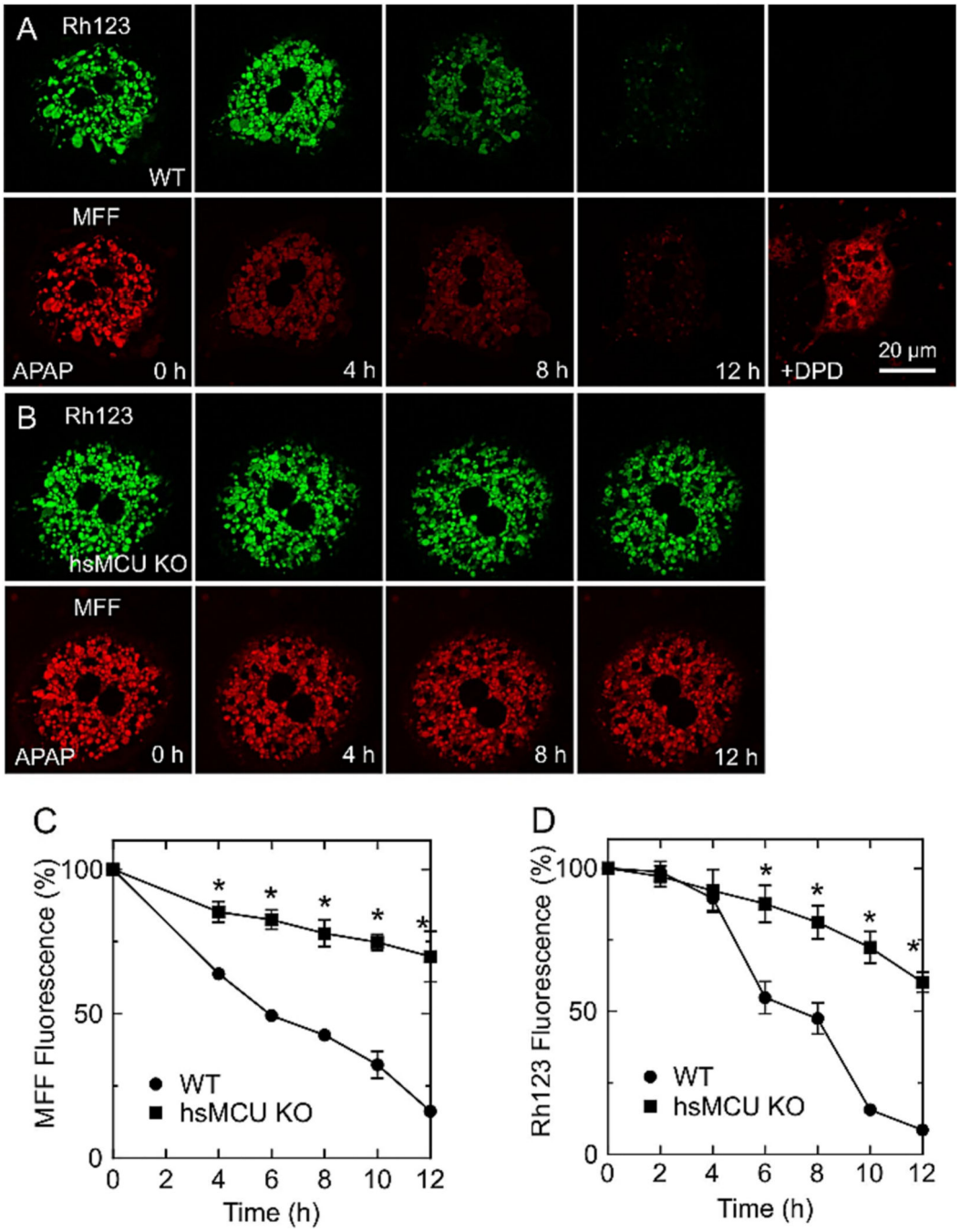

Fig. 5. Suppression of mitochondrial iron uptake and depolarization in hepatocyte specific MCU-deficient hepatocytes after acetaminophen treatment.

WT and hsMCU KO hepatocytes were exposed to 10 mM APAP in the presence of 20 mM fructose plus 5 mM glycine to prevent cell death after APAP-induced disruption of mitochondrial metabolism. In **A** and **B**, hepatocyes were loaded with 300 nM Rh123 and 1 μM MFF for confocal imaging, as described in Materials and Methods. After 12 h, 20 mM DPD was added. In **C** and **D**, average mitochondrial MFF and Rh123 fluorescence

of individual hepatocytes after background subtraction was quantified at 4–12 h as the percentage of fluorescence at 0 h. *, $p<0.01$ vs WT (n=3 hepatocytes per group).

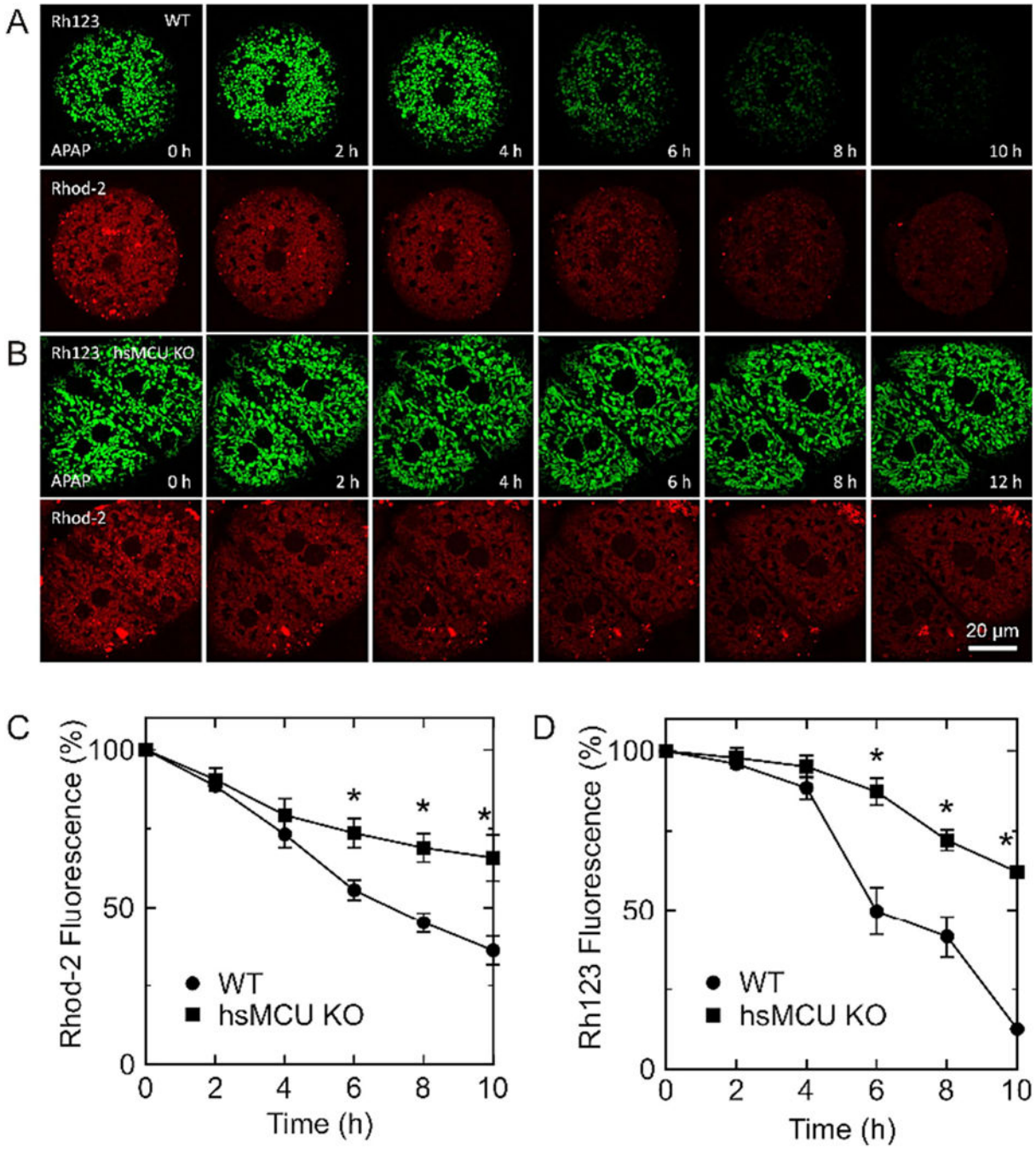

Fig. 6. Lack of an increase of mitochondrial Ca^{2+} in wildtype hepatocytes and hepatocyte specific MCU-deficient hepatocytes after acetaminophen.

Hepatocytes were exposed to 10 mM APAP as described in Fig. 5. In **A** and **B**, hepatocytes were loaded with 300 nM Rh123 and 10 μM Rhod-2 AM for confocal imaging before APAP, as described in Materials and Methods. In **C** and D, average mitochondrial Rhod-2 and Rh123 fluorescence of individual hepatocytes after background subtraction was quantified at 2–10 h as the percentage of fluorescence at 0 h. *, $p<0.05$ vs WT (n=3 hepatocytes per group).

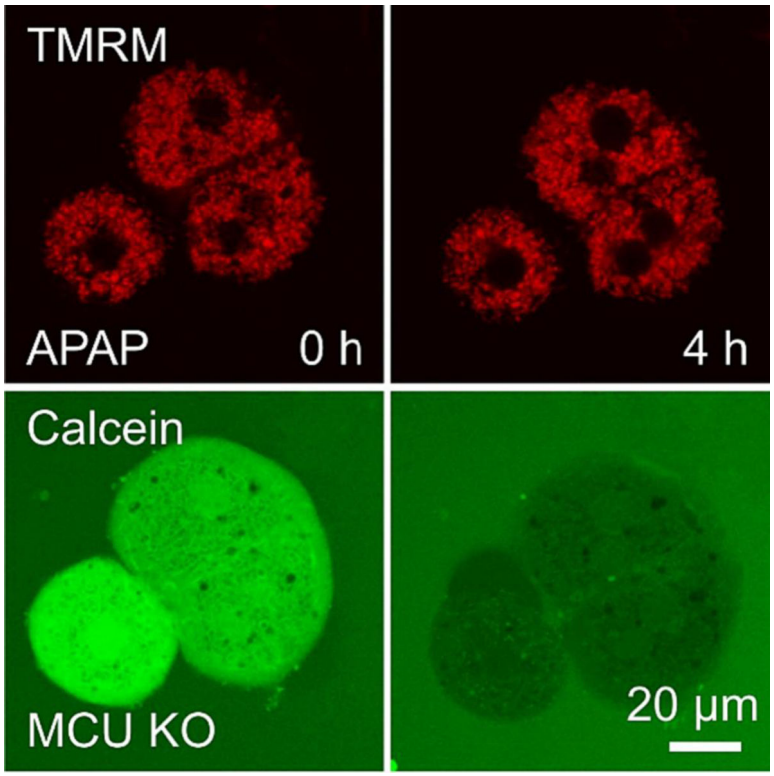

Fig 7. Increased cytosolic Fe^{2+} in MCU-deficient hepatocytes after acetaminophen.

Hepatocytes were exposed to 10 mM APAP as described in Fig. 5. Hepatocytes were loaded with 300 nM TMRM and 1 μM Calcein-AM before APAP and then incubated in the presence of 300 μM calcein-free acid for confocal imaging, as described in Materials and Methods.

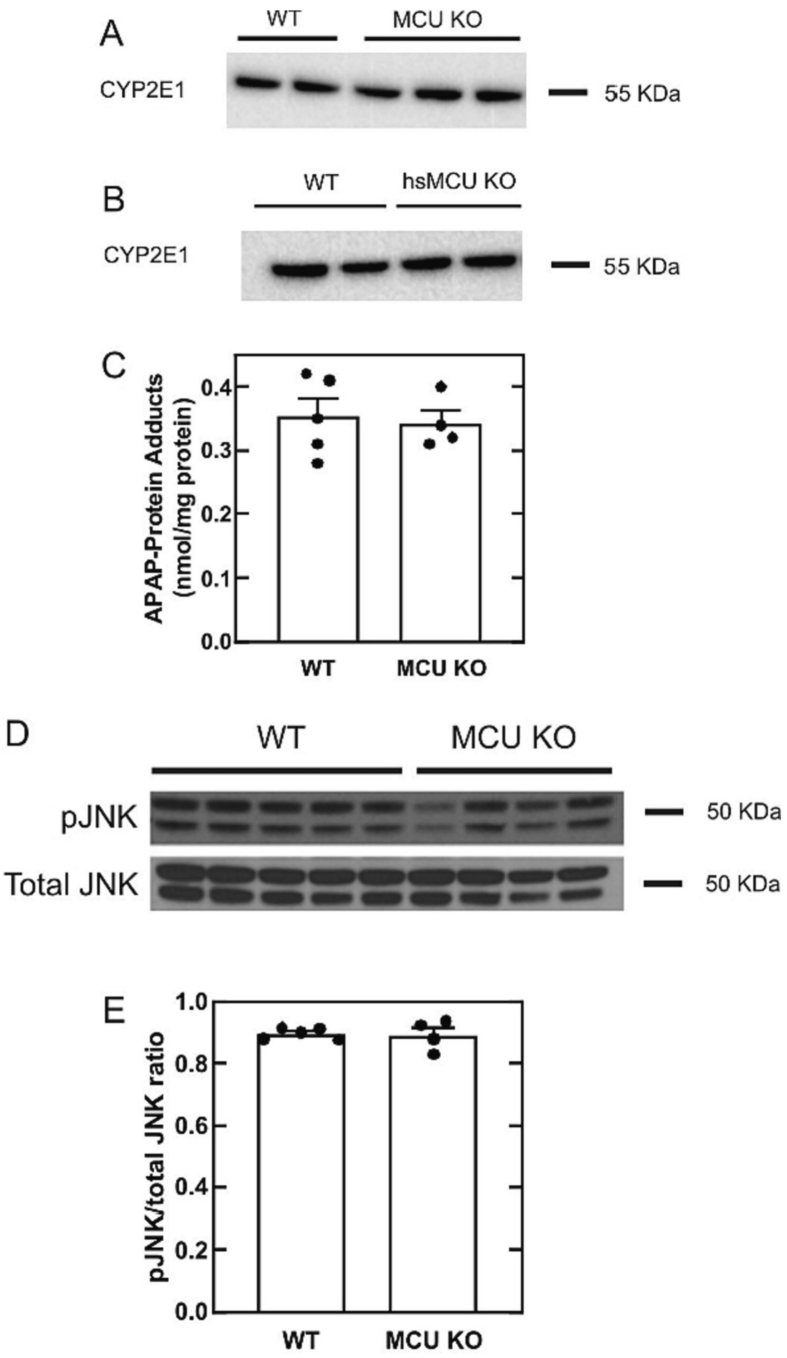

Fig. 8. Unchanged acetaminophen metabolism after MCU depletion.

Mice were administered 300 mg/kg APAP or vehicle, as described in Materials and Methods. Livers were harvested after 2 h. **A**, CYP2E1 expression was detected by Western blotting. Shown is a representative blot of CYP2E1 in WT and global MCU KO mouse liver tissue. **B**, a representative blot of CYP2E1 in WT and hsMCU KO mouse liver tissue is shown. **C**, APAP-protein adducts were measured by HPLC. **D**, JNK and p-JNK were detected by Western blotting. **E**, p-JNK/JNK ratios were determined by densitometry. Values are means ± SE (n= 3–5/group).

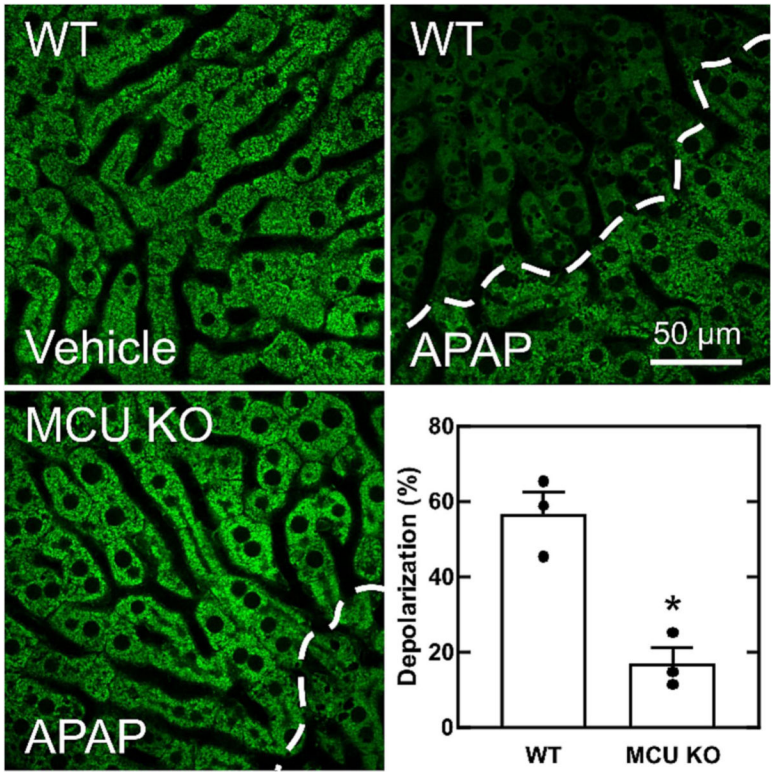

Fig. 9. Decreased mitochondrial depolarization after acetaminophen in MCU deficient compared to wildtype mice.

Mice were administered 300 mg/kg APAP or vehicle. At 24 h after APAP, Rh123 was infused, and hepatic Rh123 fluorescence was visualized by intravital multiphoton microscopy, as described in Materials and Methods. Shown are representative images of WT mice treated with vehicle (top left), WT mice treated with APAP (top right), and MCU KO mice treated with APAP (bottom left). Bar is 50 μm. Punctate labeling of Rh123 signifies mitochondrial polarization, whereas dim and diffuse cellular staining denotes mitochondrial depolarization. White dashed lines denote the border between hepatocytes with polarized and depolarized mitochondria. In bottom right, the average percentage of hepatocytes with depolarized mitochondria is plotted from 10 random fields for 3 livers per group. Depolarization was absent in vehicle-treated livers and is not plotted. *$p < 0.01$ vs. WT.